Applied Surface Science 608 (2023) 155136

Contents lists available at ScienceDirect

Applied Surface Science

journal homepage: www.elsevier.com/locate/apsusc

Full Length Article

Ti_3C_2 MXene assembled with TiO_2 for efficient photocatalytic mineralization of gaseous o-xylene

Hongyun Xue [a,b], Qiuyang Yan [a,b], Lu Chen [a,c], Yan Wang [a], Xiaofeng Xie [a], Jing Sun [a,*]

[a] State Key Lab of High Performance Ceramics and Superfine Microstructure, Shanghai Institute of Ceramics, Chinese Academy of Sciences, 1295 Dingxi Road, Shanghai 200050, China
[b] University of Chinese Academy of Sciences, 19 (A) Yuquan Road, Beijing 100049, China
[c] School of Materials Science and Engineering, Zhengzhou University, Zhengzhou 450001, China

ARTICLE INFO

Keywords:
Photocatalysis
TiO_2
Ti_3C_2
Mineralization efficiency
O-xylene

ABSTRACT

In the research of photocatalytic removal of VOCs, the mineralization rate of organic pollutants has been ignored. High mineralization rate means the reduction of intermediates, which is more conducive to environmental protection and photocatalysts stability. In this work, we successfully compounded conductive Ti_3C_2 with TiO_2 for photocatalytic degradation of o-xylene. The production of CO_2 by 1 % Ti_3C_2-TiO_2 composite was about twice than that of pure TiO_2. The results of PL and photocurrent response showed that 1 % Ti_3C_2-TiO_2 composite had less carrier recombination and higher photocurrent response, which endows its stronger photocatalytic oxidation ability than TiO_2. The in-situ infrared spectroscopy revealed that more aromatic anhydride species deposited on the TiO_2 surface and led to the less mineralization degree for TiO_2 sample. The four-cycle tests further confirmed the better stability of 1 % Ti_3C_2-TiO_2 sample. This work disclosed the role of Ti_3C_2 in enhancing the mineralization of VOCs, which may provide a new perspective for the design of high-efficiency photocatalysts.

1. Introduction

Volatile organic compounds (VOCs), including halogenated hydrocarbons, aldehydes, aromatics, ketones, olefins, ethers, etc., are considered to be among the major contributors to air pollution [1,2]. VOCs are mostly emitted from industrial production, combustion of automobile fuel and volatilization of decoration paint [3]. Most VOCs are toxic, would destroy the ecological environment and are harmful to human health [4]. So far, many VOCs control technologies have been devised. Among them, photocatalytic oxidation is one of the mainstream technologies, which is an efficient and feasible method to convert VOCs into carbon dioxide and water under ambient conditions [5,6]. Titanium dioxide, as a typical semiconductor photocatalyst, is widely used in photocatalytic degradation of VOCs because of its low-cost, nontoxicity and chemical stability [7–9].

However, most reports on photocatalytic degradation of VOCs focused on the removal efficiency of the target pollutants [10]. There are few studies on the mineralization of VOCs, which is also an important factor affecting the practical application of photocatalysts. VOCs are converted to harmless CO_2 and H_2O as much as possible, which can avoid the production of toxic intermediates in the reaction process. Some reports have revealed that highly toxic intermediates were formed in the process of photocatalytic degradation of VOCs, such as aromatic oxides, epoxides, peroxides and polyhydroxy compounds [11]. The highly toxic intermediates could cause more serious harm to the ecological environment and human health. Furthermore, the intermediates would be deposited on the surface of the photocatalysts and cover the active sites, resulting in the deactivation of photocatalysts [12]. The photocatalyst deactivation is more common in the degradation benzene series due to the high ring opening energy [13]. Therefore, it is particularly important to reduce the production of intermediates and improve the mineralization rate.

Two dimensional (2D) materials have great application potential in the field of materials science because of their excellent conductivity, high optical transparency and large specific surface area [14]. Two-dimensional materials can be directly used as catalysts for pollutant removal, or as support materials to enhance the separation of charge carrier pairs [15–17]. Among them, 2D transition metal carbonitrides (abbreviated as MXenes) are popular in recent years, which has attracted extensive attention of researchers. MXenes were obtained from MAX precursors by selective etching and exfoliation process. $Ti_3C_2T_x$ with accordion-like structure is usually used as flexible electronic device

* Corresponding author.
E-mail address: jingsun@mail.sic.ac.cn (J. Sun).

https://doi.org/10.1016/j.apsusc.2022.155136
Received 31 May 2022; Received in revised form 24 September 2022; Accepted 28 September 2022
Available online 1 October 2022

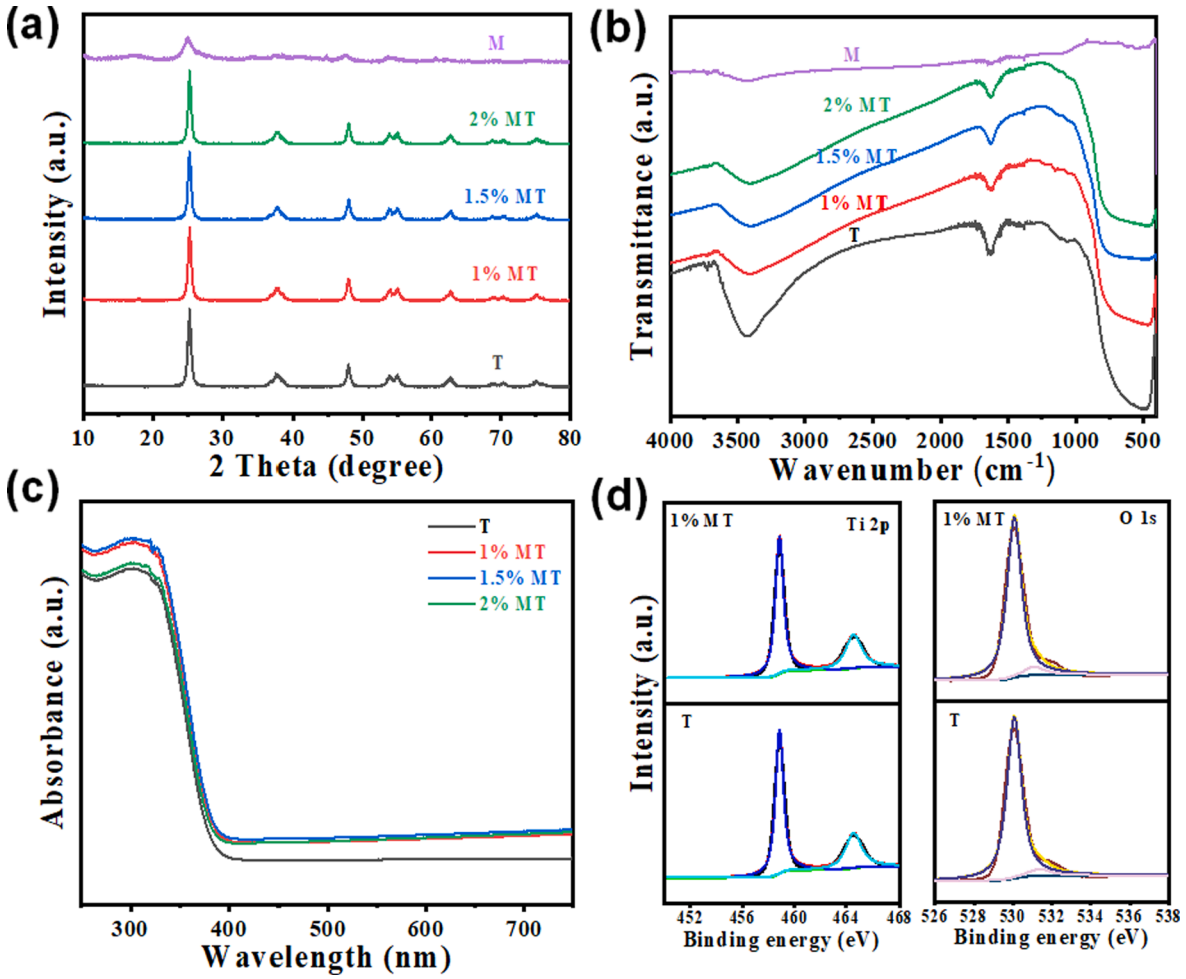

Fig. 1. (a) XRD patterns and (b) FT-IR spectra of TiO_2 (Abbreviation: T), Ti_3C_2 (Abbreviation: M) and x% Ti_3C_2-TiO_2 (Abbreviation: MT). (c) UV–vis absorption spectra of TiO_2 and x% Ti_3C_2-TiO_2. (d) XPS spectra of Ti 2p and O 1 s for 1 % Ti_3C_2-TiO_2 and TiO_2.

material or cocatalyst due to its good conductivity and unique layered structure [18]. Some reviews summarized the combination of MXenes and common photocatalysts to achieved excellent photocatalytic performance [19–21]. For example, Wang et al. synthesized the Ti_3C_2/Ti^{3+}-TiO_2 composites with mosaic structures and photodegraded acetaldehyde under visible light [22]. Li et al. reported that the photocatalytic hydrogen evolution of 1T-WS_2@TiO_2@Ti_3C_2 was 50 times higher than that of TiO_2 nanosheet. The conductive Ti_3C_2 MXene led to the increased electron transfer efficiency [23].

In our work, Ti_3C_2-TiO_2 composites were synthesized by electrostatic self-assembly for the photocatalytic degradation of gaseous o-xylene. The photodegradation efficiency of the 1 % Ti_3C_2-TiO_2 composites were slightly increased, while the mineralization rate of gaseous o-xylene was about doubled compared to that of pure TiO_2. The four-cycle experiments also shown that the composites had better stability. We further explored the surface species of photocatalysts and the effect of intermediates after degradation. Several experiments revealed that the introduction of Ti_3C_2 promoted the separation of photogenerated carriers, which improved the catalytic ability of sample and led to the reduction of intermediates in the photocatalytic process. This work focused on the mineralization rate in the process of photocatalytic degradation of VOCs and provided a method to obtain efficient photocatalysts.

2. Experimental

2.1. Chemicals and materials

Anatase titanium dioxide (TiO_2) was purchased from Aladdin Industrial Corporation. The precursor material Ti_3AlC_2 powder (200 meshes) was purchased from Forsman Scientific Corporation (China). HCl was purchased from Shanghai Titan Scientific Co., Ltd. LiF was purchased from Sinopharm Chemical Reagent Co., Ltd. Deionized water was produced by a Milli-Q system (R > 18.1 MΩ). O-xylene standard gas (20 ppm) was provided by Shanghai Weichuang Standard Gas Analytical Technology Co. Ltd.

2.2. Preparation of Ti_3C_2

In a typical synthesis, 50 ml HCl, 17 ml deionized water and 6 g LiF were added into Teflon beaker successively and stirred about 15 min. Then 3 g Ti_3AlC_2 was added into beaker and transferred to the oil bath pot. After the heat treatment for 48 h, the sample was washed with 1000 ml deionized water and centrifuged several times. The sediment was obtained by filtration and freeze-dried for 12 h. Afterward, 1 g dried sediment was added into 50 ml deionized water and ultrasonic for 120 min in Ar atmosphere to exfoliate the Ti_3C_2 MXene nanosheets. Centrifugation for 1 h (rotational speed 3500 r/min) was performed to collect the supernatant. The supernatant was freeze-dried to obtain 2D Ti_3C_2 MXene, named as M.

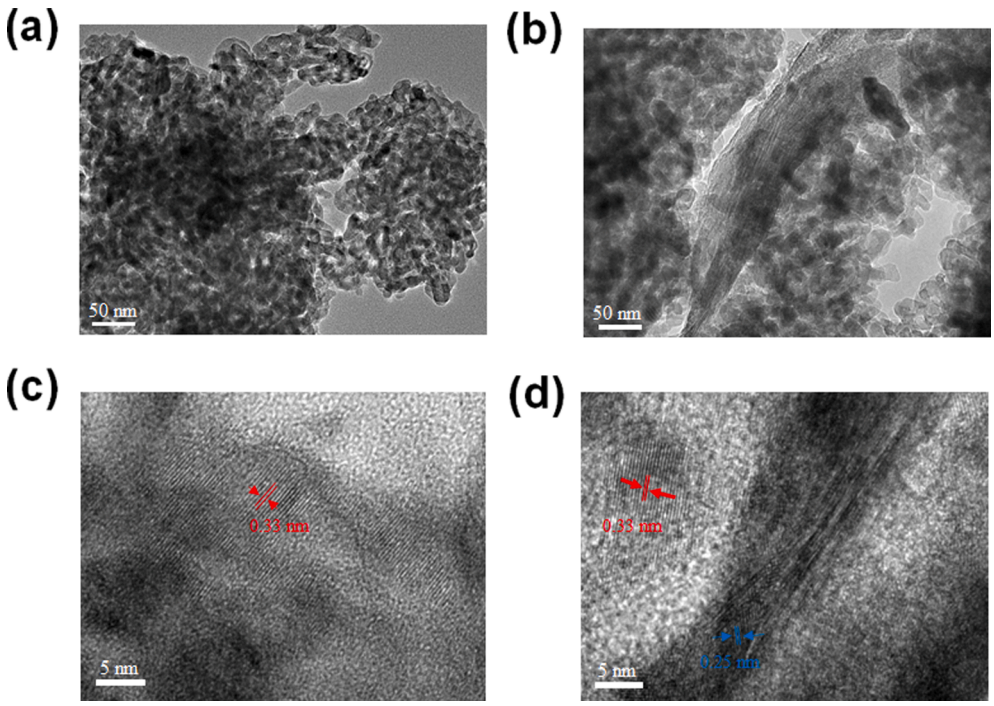

Fig. 2. TEM and HRTEM images of (a, c) TiO_2 and (b, d) 1 % Ti_3C_2-TiO_2.

2.3. Preparation of Ti_3C_2-TiO_2 composites

Firstly, the commercial anatase titanium dioxide was calcined at 350 °C for 2 h to remove the surface organic matter, named as T. The layered Ti_3C_2 was ultrasonically dispersed in 50 ml deionized water. The obtained dispersion was compounded with TiO_2 by electrostatic self-assembly method, stirred for 24 h. After that, the mixed suspension was centrifuged and then vacuum dried at 80 °C for 15 h. The samples were named as x% MT, where the x% represented the mass percentage of Ti_3C_2.

2.4. Characterization

X-ray diffraction (XRD) spectra were carried out by a high-resolution power X-ray diffractometer (D8 advance, Bruker, Germany) using Cu Ka radiation ($\lambda = 0.154$ nm) and the diffraction angle range was 10–80° (5°/min). Raman spectra were tested by a DXR Raman Microscope (Thermal Scientific corporation, USA). Fourier transform infrared (FTIR) spectra were collected by a NICOLET ls 10 infrared spectrophotometer with a KBr pellet technique. UV–vis diffuse reflectance spectra were measured on a Shimadzu UV-3600 spectrometer (lambda 950, PerkinElmer, USA) by using $BaSO_4$ as reference. Transmission electron microscopy (TEM) images were obtained on JEM-2100F transmission electron microscope. X-ray photoelectron spectroscopy (XPS) was measured by a ESCAlab250 (Thermo Fisher Scientific) instrument. Photoluminescence spectra were tested by an Edinburgh Instruments FLSP-920 (ls-55, PerkinElmer, USA) fluorescence spectrophotometer with an excitation wavelength of 320 nm. The photo electrochemistry tests were used CHI660D electrochemical workstation (Chenhua Instrument Co., Ltd., China). Before the test, the samples were dispersed in ethanol solution and ball-milled for 8 h. Then the slurry was spin coated on F-doped SnO_2 conductive glass (FTO) as working electrode. The platinum plate as counter electrode, while the Ag/AgCl as reference electrode. The approximate distance between Xenon lamp and photoelectrode was 20 cm.

2.5. Photocatalytic performance tests

10 ppm o-xylene was represented as the target pollutant and a 300 W Xenon lamp was used as the light source. 100 mg of sample was dispersed in ethanol, and then the suspension coated on the glass plate (15 * 7.5 * 0.3, cm), and was placed in the reaction chamber. The distance from the light source was set to 30 cm. The flow rate was set to 40 standard cubic centimeter per minute (sccm) through the flow control system. The concentration of o-xylene at the outlet was monitored in real time by gas chromatograph (GC), and the data was collected every 10 min. The photodegradation efficiency of gaseous o-xylene was estimated by $X = (C_0\text{-}C)/C_0 \times 100$ %, where C_0 (ppm) and C (ppm) represented the original concentration and different time interval concentration of gaseous o-xylene, respectively. The mineralization rate of gaseous o-xylene was calculated by $\eta = \triangle[CO_2]/(8 \times C_{in}) \times 100$ %, where $\triangle[CO_2]$ is the outlet CO_2 concentrations, C_{in} is the inlet concentration of gaseous o-xylene, and $(8 \times C_{in})$ represented the theoretical yield of CO_2 produced when o-xylene was completely oxidized.

In-situ diffuse reflectance infrared Fourier transform spectroscope (Shimadzu Co., Ltd, China) was used to analyze the surface state of samples during photocatalytic reaction. Firstly, the sample was filled in a mold with nickel mesh and fixed in the salt window of the reaction tank. Next, high-purity N_2 was injected to remove the impurity gas in the pipeline and reaction tank. After 20 min, then N_2 was turned off and the instrument was turned on to collect the background substrate. After that, the mixed gas of o-xylene and air was inlet into reaction tank, and the timer started counting at the same time. The data was collected every 3 min to monitor the organic matter on the sample surface in real time. The adsorption was carried out for 150 min in the dark.

3. Results and discussion

The phase structure of Ti_3C_2, TiO_2 and Ti_3C_2-TiO_2 composites were shown in Fig. 1a. The XRD spectra presented that the regular structure of anatase TiO_2 in the Ti_3C_2-TiO_2 composites still be maintained, which indicated that Ti_3C_2 had little influence on the crystallinity of TiO_2. Fig. 1b displayed the Fourier transform infrared spectroscopy (FT-IR) of the as prepared photocatalysts. The peaks at 500 cm^{-1}(O—Ti—O), 1630

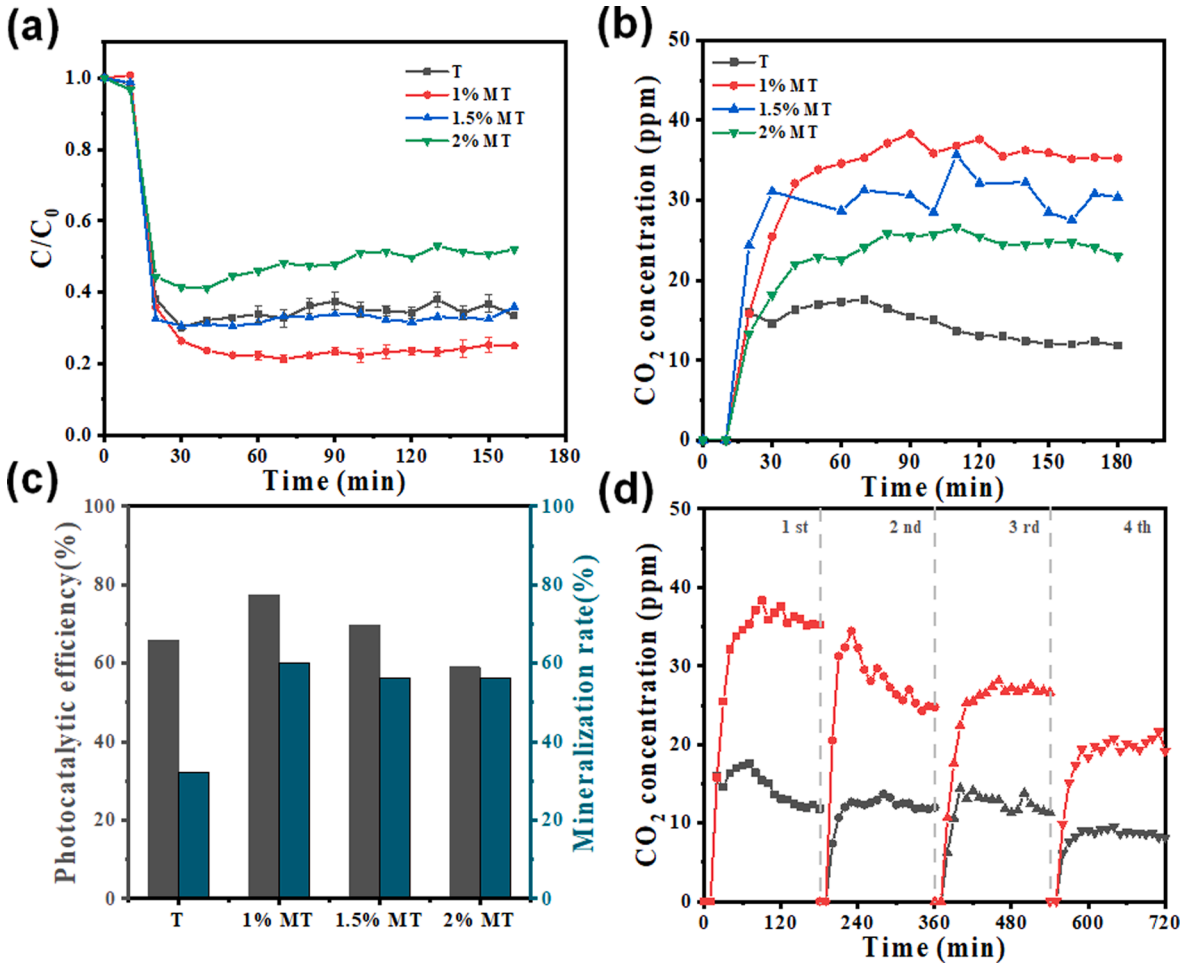

Fig. 3. (a) The photocatalytic degradation and (b) CO_2 generation curves of gaseous o-xylene with photocatalysts illuminated by 300 W Xenon lamp. (c) Histograms of photocatalytic efficiency and mineralization rate of samples. (d) The CO_2 concentration produced during photodegradation of o-xylene with TiO_2 (black line) and1 % Ti_3C_2-TiO_2 (red line) under continuous irradiation for four cycles.

cm^{-1}(C═O), 3440 cm^{-1}(O—H) were assigned to the pristine TiO_2 due to the adsorption of CO_2 and H_2O molecules on the surface. The introduction of Ti_3C_2 weakened the peak intensity of ν(C═O) and ν(O—H), indicating that the combination of Ti_3C_2 and TiO_2 hindered the adsorption of CO_2 and H_2O. UV–vis diffuse reflectance spectra (Fig. 1c) showed that the absorption edges of the Ti_3C_2-TiO_2 composites were not shifted, which meant that the band gap of composites did not change. An enhancement of UV–vis absorption was observed in the composites. XPS spectra further revealed the interaction of the components. As shown in the Fig. 1d, the O 1s peak located at about 530.07 eV and 531.35 eV corresponding to the lattice oxygen and oxygen of surface hydroxyl, respectively. The Ti 2p peak at about 458.4 eV and 464.55 eV corresponding to the Ti 2p3/2 and Ti 2p1/2, respectively. The electronic structure of the composites had not changed significantly.

The microstructure was characterized by TEM and high-resolution TEM (HRTEM). TEM images in Fig. 2a, b exhibited that TiO_2 presented uniform small particles, while Ti_3C_2 had a thin-layer structure. The HRTEM image of TiO_2 showed a clear lattice fringe with an interplane spacing of 0.33 nm, which was consistent with (1 1 0) planes. An interlayer space of 0.25 nm could be observed in the HRTEM image of 1 %Ti_3C_2-TiO_2 samples, corresponding to the (0 0 6) facet of Ti_3C_2 [24]. The zeta potential of TiO_2 and Ti_3C_2 were positive (5.59 mV) and negative (−35.53 mV), respectively. The TiO_2 and Ti_3C_2 were assembled together by electrostatic attraction.

The photodegradation performance of the photocatalysts were shown in Fig. 3a. After reaching adsorption equilibrium, the concentration of pollutants decreased rapidly when turning on the light, and finally the degradation rate tended to be stable. The removal efficiency of o-xylene over TiO_2, 1 % Ti_3C_2-TiO_2, 1.5 % Ti_3C_2-TiO_2 and 2 % Ti_3C_2-TiO_2 was 65.7 %, 77.3 %, 69.5 % and 59.0 %, respectively. As can be seen from the repeated test results (Fig. S1, Table S1 and S2), the degradation efficiency of TiO_2 and 1 % Ti_3C_2-TiO_2 had good repeatability. The standard error (S.E.) was calculated by formula $\sigma = \sqrt{\frac{\sum (X_i - X)^2}{n}}$ (X is the arithmetic mean). The average error range of the degradation efficiency of TiO_2 and 1 % Ti_3C_2-TiO_2 was 2.1 % and 1.5 %, respectively. Although the photocatalytic degradation of 1 % Ti_3C_2-TiO_2 was slightly better than that of TiO_2, surprisingly more thorough mineralization occurred on samples with Ti_3C_2. As shown in Fig. 3b, the CO_2 concentration increased gradually after irradiation. CO_2 yield of 37 ppm for 1 % Ti_3C_2-TiO_2 was higher than that (17 ppm) of TiO_2, indicating that the introduction of Ti_3C_2 enhanced the mineralization degree of o-xylene to CO_2. The mineralization rate was 32.3 %, 59.8 %, 56.2 % and 56.4 % for samples TiO_2, 1 % Ti_3C_2-TiO_2, 1.5 % Ti_3C_2-TiO_2 and 2 % Ti_3C_2-TiO_2, respectively (Fig. 3c). Deep mineralization means more o-xylene is fully oxidized into CO_2 instead of converting into other intermediates. This will help to keep the active sites of photocatalysts available instead of losing activity quickly. The stability of the two samples were compared by recycling photocatalytic reaction as shown in Fig. 3d. After four cycles, CO_2 yield for 1 % Ti_3C_2-TiO_2 was above 20 ppm, which was still much higher than that of TiO_2. The degradation efficiency of 1 % Ti_3C_2-TiO_2 remained about 50 % was also higher than

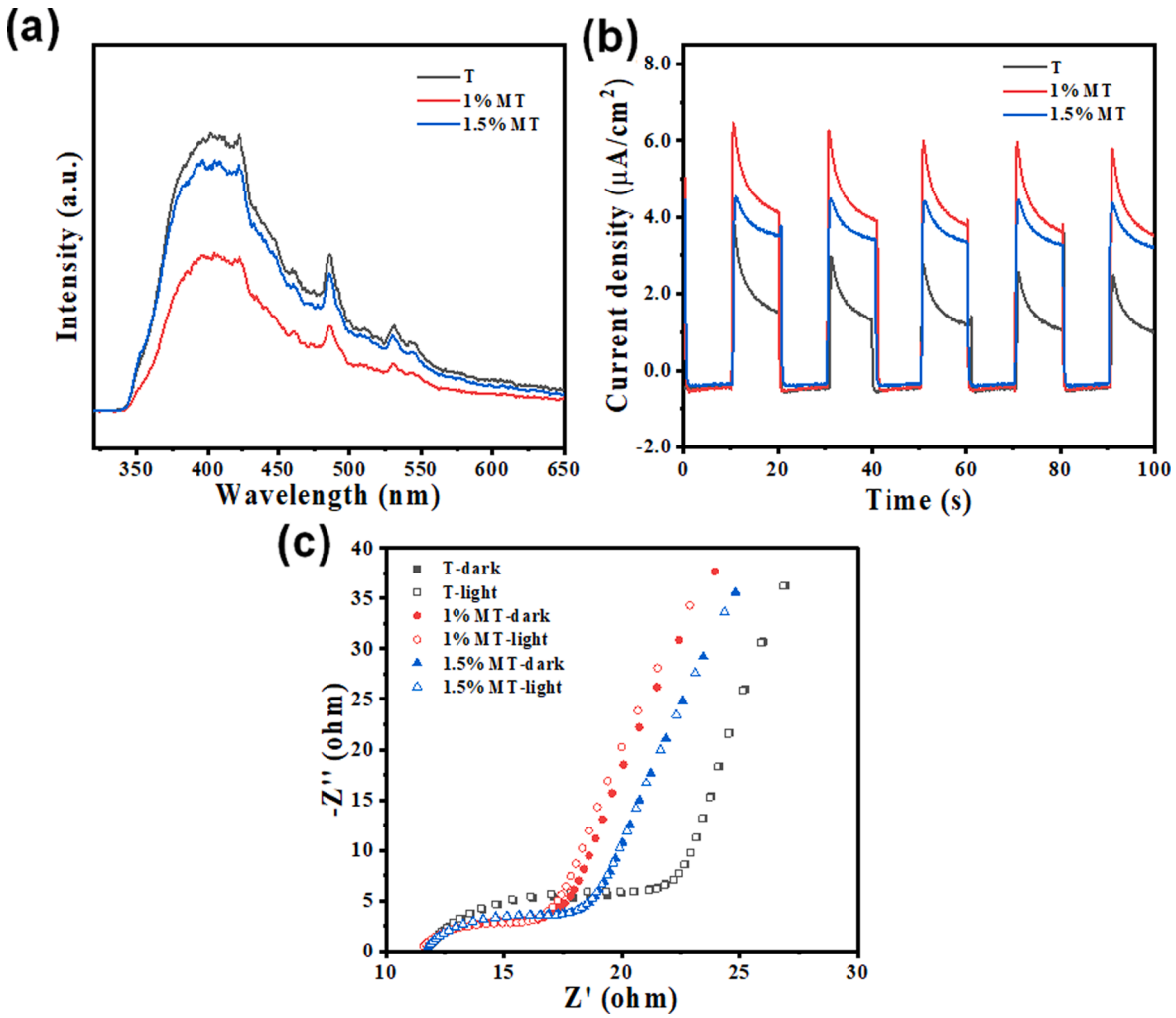

Fig. 4. (a) PL spectra, (b) photocurrent response and (c) EIS spectra of TiO_2, 1 % Ti_3C_2-TiO_2 and 1.5 % Ti_3C_2-TiO_2.

that of TiO_2 after four cycles (Fig. S2). Thus, the 1 % Ti_3C_2-TiO_2 sample exhibited better stability than pure TiO_2.

In order to understand the connection between the intrinsic properties of samples and their decomposing behaviors, photoluminescence spectra and photoelectrochemistry tests were carried out to characterize TiO_2, 1 % Ti_3C_2-TiO_2 and 1.5 % Ti_3C_2-TiO_2. Generally, the lower the PL intensity denotes the weaker recombination of photogenerated carriers. The PL intensities of Ti_3C_2-TiO_2 composites were much lower compared to that of pure TiO_2. And the PL intensity of the 1 % Ti_3C_2-TiO_2 was the lowest. The higher photocurrent response represents higher charges density and more effective migration of photogenerated carriers. The TiO_2, 1 % Ti_3C_2-TiO_2 and 1.5 % Ti_3C_2-TiO_2 had similar dark current density, about −0.46 μA/cm^2. The photocurrent density of TiO_2, 1 % Ti_3C_2-TiO_2 and 1.5 % Ti_3C_2-TiO_2 was about 2.08 μA/cm^2, 4.55 μA/cm^2 and 3.77 μA/cm^2, respectively. Ti_3C_2-TiO_2 composites exhibited higher photocurrent responses signal, which indicated that the introduction of Ti_3C_2 promoted the production and migration of photogenerated charges. Especially, the 1 % Ti_3C_2-TiO_2 sample shown the maximum current density increment. The reduction of the diameter of the semi -arc diameter in the EIS diagram indicates that the resistance of the electrode and the electrolyte interface is reduced. As shown in Fig. 4c, compared with TiO_2 electrode, the semicircle diameter of the Ti_3C_2-TiO_2 composites electrodes decreased, indicated that Ti_3C_2 could significantly enhance charge transfer. At the same time, the results of the Bode phase plot were shown in Fig. S3, which can be used to calculate the electron lifetime in the materials [25]. The lifetime of TiO_2, 1 % Ti_3C_2-TiO_2 and 1.5 % Ti_3C_2-TiO_2 was 40.8 μs, 50.2 μs and 50.2 μs, respectively. The introduction of Ti_3C_2 enhanced the charge separation efficiency. The results of PL and photoelectrochemistry tests confirmed that more photogenerated electrons were involved in the degradation of o-xylene for 1 % Ti_3C_2-TiO_2. Therefore, the 1 % Ti_3C_2-TiO_2 showed the best performance (see Fig. 3c).

The *in-situ* DRIFTS measurement was employed to dynamically monitor the changes of intermediates on the surface of the photocatalysts during the adsorption and degradation process. At the beginning of adsorption, the stretching vibration peak of benzene ring appeared at 1400–1647 cm^{-1}. The bands at the 3070 cm^{-1} and ~ 2870 cm^{-1} were assigned to ν(C—H) of the aromatic ring and the methyl group, respectively [26]. The negative peaks at 3660, 3740 cm^{-1} were assigned to the stretching vibration of surface OH species [27]. After turning on the light, an obvious new band was generated at ~ 1735 cm^{-1}, which was referred as the ν(C═O) vibration of aromatic aldehyde. And the intensity of the peak was gradually increasing. The peak at 1300 cm^{-1} was attributed to C—O—C stretching vibration of the anhydride species [27]. With the extension of reaction time, the peaks of these intermediates enhanced, indicated their accumulation on photocatalysts. Compared to 1 % Ti_3C_2-TiO_2 composite, the peaks intensities of anhydride species (1740, 1296 cm^{-1}) were more obvious in the TiO_2 sample (1735, 1307 cm^{-1}). It can be inferred that more aromatic anhydride species accumulated on the surface of TiO_2 during photocatalytic degradation of o-xylene, which explained the less mineralization for TiO_2 sample than 1 % Ti_3C_2-TiO_2 composite.

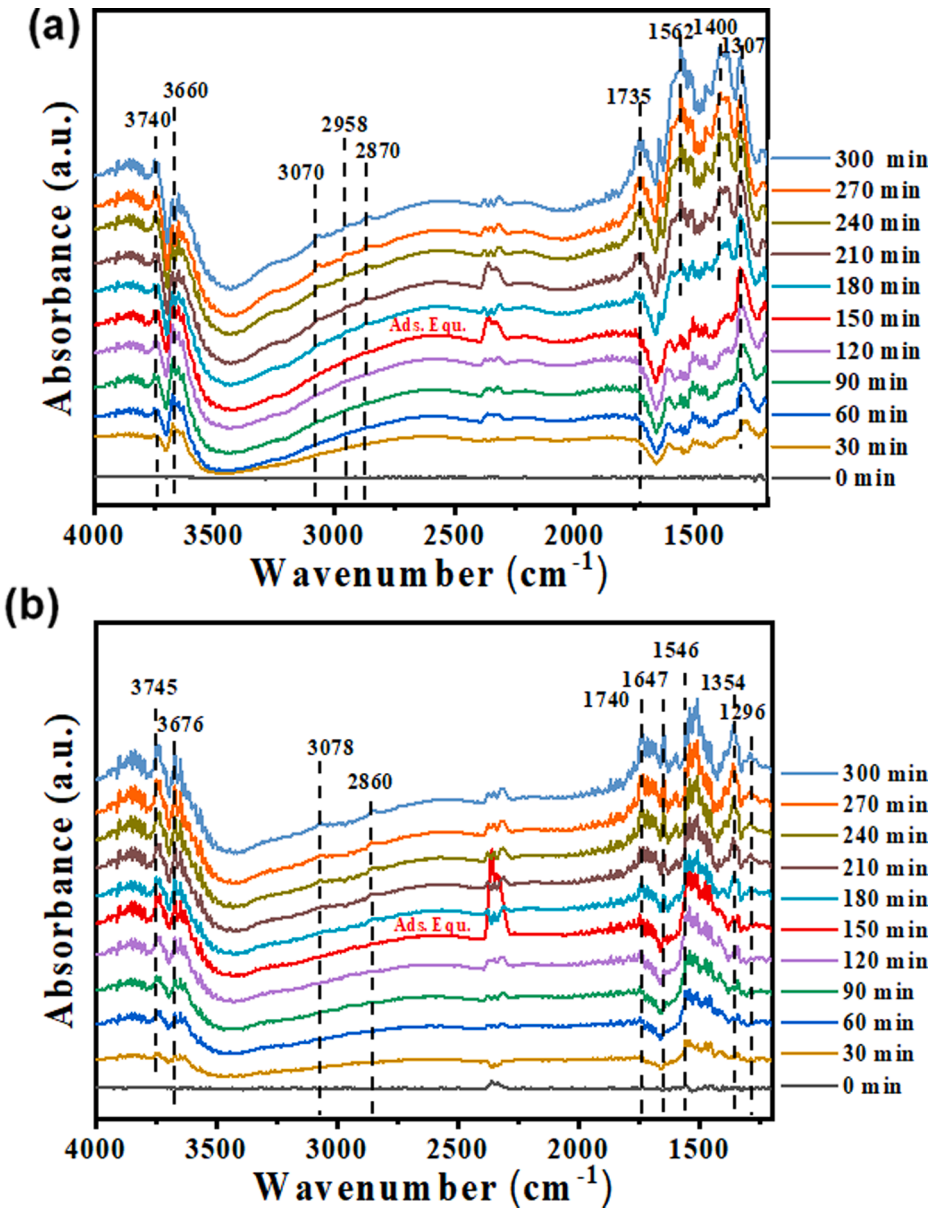

Fig. 5. In situ DRIFTS spectra of adsorption and photocatalytic degradation processes of gaseous o-xylene over (a) TiO_2 and (b) 1 % Ti_3C_2-TiO_2 surface.

In order to further explore the influence of intermediates on the performance of the photocatalyst, a series of experiments, including XRD Raman, PL and photocurrent were carried out as shown in Fig. 6. XRD spectra showed that the phase structure of the samples after four-cycles did not change significantly, which indicated that the crystal structure of the photocatalysts were not destroyed before and after the reaction. The Raman spectra shown that there was a bulged peak at 1500 cm^{-1}, which confirmed the formation of carbonaceous sediments. Moreover, the bulged peak intensity of 1 % Ti_3C_2-TiO_2 composite was lower than that of TiO_2, indicating that the intermediates on the surface of 1 % Ti_3C_2-TiO_2 were fewer. As shown in Fig. 6c and d, the TiO_2 and 1 % Ti_3C_2-TiO_2 after four cycles both exhibited lower PL intensity than fresh TiO_2 and 1 % Ti_3C_2-TiO_2. The results of photocurrent responses in Fig. 6e and f were consistent with that of PL. The essential reason may be that the accumulation of intermediates led to the coverage of active sites and hindered the generation of photogenerated carriers. However, the photocurrent responses of TiO_2 sample decreased more obviously than that of 1 % Ti_3C_2-TiO_2, which indicated that the 1 % Ti_3C_2-TiO_2 produced less intermediates. The increased mineralization rate and the less intermediates for 1 % Ti_3C_2-TiO_2 contribute the enhanced photocatalytic performance.

4. Conclusions

In summary, we successfully synthesized a series of TiO_2 coupling with Ti_3C_2 for photocatalytic degradation of gaseous o-xylene. The composites showed superior photocatalytic degradation performance and the capability of mineralization. The mineralization degree of 1 % Ti_3C_2-TiO_2 composites was about twice than that of pure TiO_2. The PL and photocurrent experiments revealed that 1 % Ti_3C_2-TiO_2 sample exhibited lower recombination of charged carriers and higher photocurrent response in comparison to pure TiO_2, which meant the 1 % Ti_3C_2-TiO_2 possessed stronger photocatalytic oxidation ability. The results of in-situ infrared spectra revealed that more aromatic anhydride species accumulated on the surface of TiO_2, which led to the reduction of photogenerated carries. The four-cycle experiments also proved that the photocatalytic activity of 1 % Ti_3C_2-TiO_2 sample was much better than that of pure TiO_2. In our work, the composite photocatalysts reduced the production of toxic intermediates and preserved the active sites for better stability. This work provides a reference for improving the

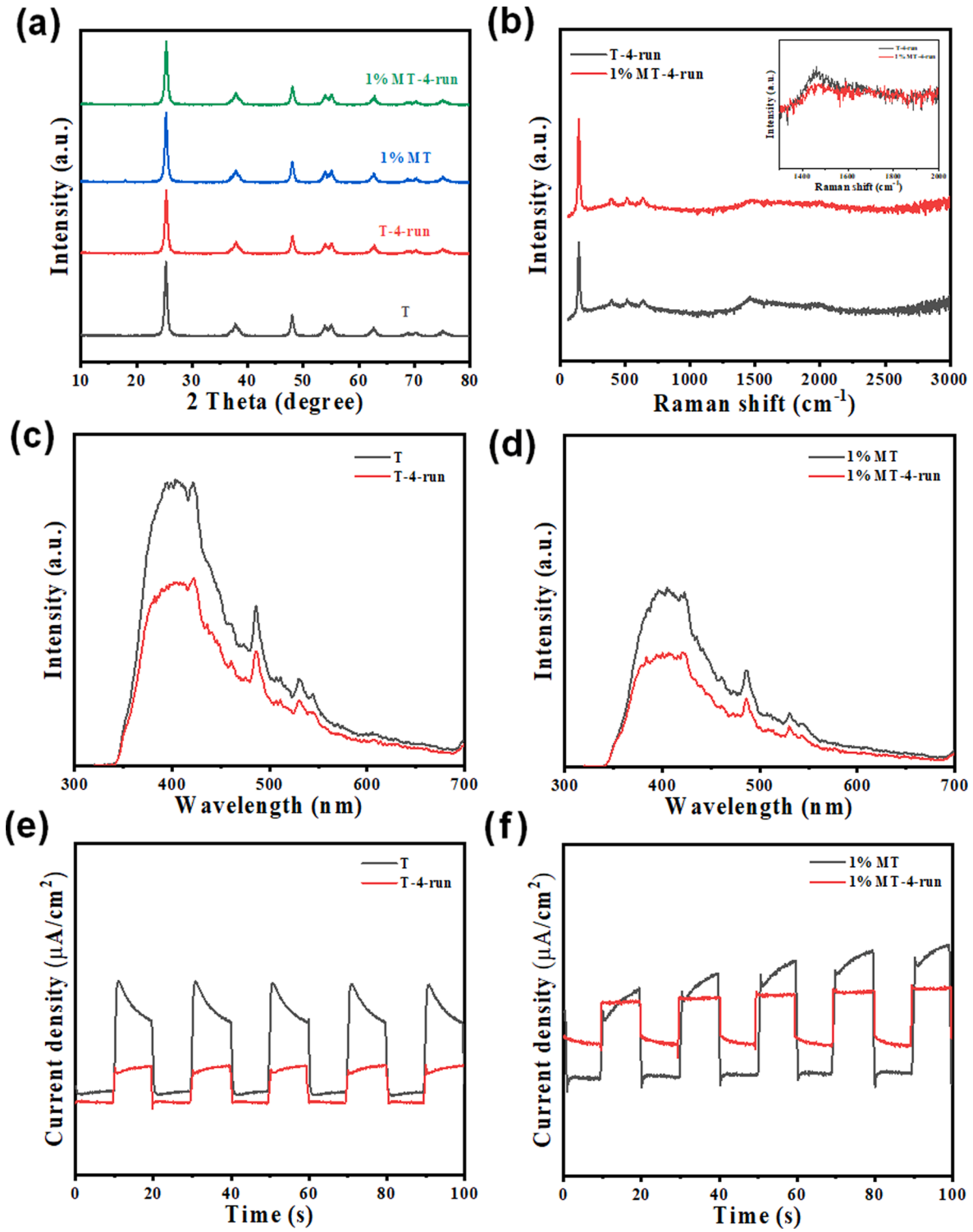

Fig. 6. (a) XRD patterns of TiO_2 and 1 % Ti_3C_2-TiO_2 before and after four cycles. (b) Raman spectra of TiO_2 and 1 % Ti_3C_2-TiO_2 after four cycles. PL spectra for samples (c) TiO_2 and (d) 1 % Ti_3C_2-TiO_2 as prepared and after four degradation experiments. Photocurrent curves for samples (e) TiO_2 and (f) 1 % Ti_3C_2-TiO_2 as prepared and after four degradation experiments.

mineralization ability of the photocatalysts and further promote the design of photocatalysts with high efficiency.

CRediT authorship contribution statement

Hongyun Xue: Conceptualization, Investigation, Methodology, Formal analysis, Data curation, Writing – original draft. **Qiuyang Yan:** . **Lu Chen:** Formal analysis, Investigation. **Yan Wang:** Project administration, Funding acquisition. **Xiaofeng Xie:** Validation, Supervision, Project administration, Funding acquisition. **Jing Sun:** Conceptualization, Methodology, Resources, Funding acquisition, Project administration, Validation, Supervision, Writing – review & editing.

Declaration of Competing Interest

The authors declare that they have no known competing financial interests or personal relationships that could have appeared to influence the work reported in this paper.

Data availability

Data will be made available on request.

Acknowledgment

This work was financially supported by the Key Collaborative Research Program of the Alliance of International Science Organizations, (Grant. No. ANSO-CR-KP-2020-13), the National Key Research and Development Program of China (2021YFE0110400), the State Key Laboratory Director Fund of SICCAS (Y9ZC0102).

Appendix A. Supplementary material

Supplementary data to this article can be found online at https://doi.org/10.1016/j.apsusc.2022.155136.

References

[1] M.S. Kamal, S.A. Razzak, M.M. Hossain, Catalytic oxidation of volatile organic compounds (VOCs)—A review, Atmos. Environ. 140 (2016) 117–134.
[2] C. He, J. Cheng, X. Zhang, M. Douthwaite, S. Pattisson, Z. Hao, Recent Advances in the Catalytic Oxidation of Volatile Organic Compounds: A Review Based on Pollutant Sorts and Sources, Chem. Rev. 119 (7) (2019) 4471–4568.
[3] X. Yao, Y. Liu, T. Li, T. Zhang, H. Li, W. Wang, X. Shen, F. Qian, Z. Yao, Adsorption behavior of multicomponent volatile organic compounds on a citric acid residue waste-based activated carbon: Experiment and molecular simulation, J. Hazard. Mater. 392 (2020) 122323.
[4] U. Pöschl, M. Shiraiwa, Multiphase Chemistry at the Atmosphere−Biosphere Interface Influencing Climate and Public Health in the Anthropocene, Chem. Rev. 115 (10) (2015) 4440–4475.
[5] H. Liu, Y. Ma, J. Chen, M. Wen, G. Li, T. An, Highly efficient visible-light-driven photocatalytic degradation of VOCs by CO_2-assisted synthesized mesoporous carbon confined mixed-phase TiO_2 nanocomposites derived from MOFs, Appl. Catal. B: Environ. 250 (2019) 337–346.
[6] T. Xue, R. Li, Y. Gao, Q. Wang, Iron mesh-supported vertically aligned Co-Fe layered double oxide as a novel monolithic catalyst for catalytic oxidation of toluene, Chem. Eng. J. 384 (2020) 123284.
[7] M. Pelaez, N.T. Nolan, S.C. Pillai, M.K. Seery, P. Falaras, A.G. Kontos, P.S. M. Dunlop, J.W.J. Hamilton, J.A. Byrne, K. O'Shea, M.H. Entezari, D.D. Dionysiou, A review on the visible light active titanium dioxide photocatalysts for environmental applications, Appl. Catal. B: Environ. 125 (2012) 331–349.
[8] J. Chen, G. Li, H. Zhang, P. Liu, H. Zhao, T. An, Anatase TiO_2 mesocrystals with exposed (0 0 1) surface for enhanced photocatalytic decomposition capability toward gaseous styrene, Catal. Today 224 (2014) 216–224.
[9] Y. Shu, J. Ji, Y. Xu, J. Deng, H. Huang, M. He, D.Y.C. Leung, M. Wu, S. Liu, S. Liu, G. Liu, R. Xie, Q. Feng, Y. Zhan, R. Fang, X. Ye, Promotional role of Mn doping on catalytic oxidation of VOCs over mesoporous TiO_2 under vacuum ultraviolet (VUV) irradiation, Appl. Catal. B: Environ. 220 (2018) 78–87.
[10] Z. Shayegan, C.-S. Lee, F. Haghighat, TiO_2 photocatalyst for removal of volatile organic compounds in gas phase – A review, Chem. Eng. J. 334 (2018) 2408–2439.
[11] X. Dong, W. Cui, H. Wang, J. Li, Y. Sun, H. Wang, Y. Zhang, H. Huang, F. Dong, Promoting ring-opening efficiency for suppressing toxic intermediates during photocatalytic toluene degradation via surface oxygen vacancies, Sci. Bull. 64 (10) (2019) 669–678.
[12] F. He, U. Muliane, S. Weon, W. Choi, Substrate-specific mineralization and deactivation behaviors of TiO_2 as an air-cleaning photocatalyst, Appl. Catal. B: Environ. 275 (2020) 119145.
[13] P. Chen, W. Cui, H. Wang, X. Dong, J. Li, Y. Sun, Y. Zhou, Y. Zhang, F. Dong, The importance of intermediates ring-opening in preventing photocatalyst deactivation during toluene decomposition, Appl. Catal. B: Environ. 272 (2020) 118977.
[14] X. Cai, Y. Luo, B. Liu, H.-M. Cheng, Preparation of 2D material dispersions and their applications, Chem. Soc. Rev. 47 (16) (2018) 6224–6266.
[15] S. Nayak, G. Swain, K. Parida, Enhanced Photocatalytic Activities of RhB Degradation and H_2 Evolution from in Situ Formation of the Electrostatic Heterostructure MoS_2/NiFe LDH Nanocomposite through the Z-Scheme Mechanism via p−n Heterojunctions, ACS Appl. Mater. Interfaces 11 (23) (2019) 20923–20942.
[16] S. Nayak, K. Parida, MgCr-LDH Nanoplatelets as Effective Oxidation Catalysts for Visible Light-Triggered Rhodamine B Degradation, CATALYSTS 11 (2021) 1072.
[17] S. Nayak, K.M. parida, Deciphering Z-scheme Charge transfer Dynamics in Heterostructure NiFe-LDH/NrGo/g-C3N 4 Nanocomposite for photocatalytic pollutant Removal and Water splitting Reactions, Sci. Rep. 9 (2019) 2458.
[18] L. Gao, W. Bao, A.V. Kuklin, S. Mei, H. Zhang, H. Ågren, Hetero-MXenes: Theory, Synthesis, and Emerging Applications, Adv. Mater. 33 (10) (2021) 2004129.
[19] A. Sreedhar, J.-S. Noh, Recent advances in partially and completely derived 2D Ti_3C_2 MXene based TiO_2 nanocomposites towards photocatalytic applications: A review, Sol. Energy 222 (2021) 48–73.
[20] L. Biswal, S. Nayak, K. Parida, Recent progress on strategies for the preparation of 2D/2D MXene/g-C_3N_4 nanocomposites for photocatalytic energy and environmental applications, Catal. Sci. Technol. 11 (4) (2021) 1222–1248.
[21] L. Biswal, R. Mohanty, S. Nayak, K. Parida, Review on MXene/TiO_2 nanohybrids for photocatalytic hydrogen production and pollutant degradations, J. Environ. Chem. Eng. 10 (2) (2022) 107211.
[22] X. Wang, Y. Yang, G. Lu, G. Shi, Y. Wang, R. Wang, X. Xie, J. Sun, In-situ preparation of Ti_3C_2/Ti^{3+}-TiO_2 composites with mosaic structures for the adsorption and Photo-degradation of flowing acetaldehyde under visible light, Appl. Surf. Sci. 531 (2020) 147101.
[23] Y. Li, L. Ding, S. Yin, Z. Liang, Y. Xue, X. Wang, H. Cui, J. Tian, Photocatalytic H_2 Evolution on TiO_2 Assembled with Ti_3C_2 MXene and Metallic 1T-WS_2 as Co-catalysts, Nano-Micro Lett. 12 (1) (2020).
[24] C. Peng, X. Yang, Y. Li, H. Yu, H. Wang, F. Peng, Hybrids of Two-Dimensional Ti_3C_2 and TiO_2 Exposing 001 Facets toward Enhanced Photocatalytic Activity, ACS Appl. Mater. Interfaces 8 (9) (2016) 6051–6060.
[25] S. Nayak, K. Parida, Superlative photoelectrochemical properties of 3D MgCr-LDH nanoparticles influencing towards photoinduced water splitting reactions, Sci. Rep. 12 (1) (2022).
[26] X. Li, Z. Zhu, Q. Zhao, S. Liu, FT-IR study of the photocatalytic degradation of gaseous toluene over UV-irradiated TiO_2 microballs: enhanced performance by hydrothermal treatment in alkaline solution, Appl. Surf. Sci. 257 (10) (2011) 4709–4714.
[27] Z. Rao, G. Lu, A. Mahmood, G. Shi, X. Xie, J. Sun, Deactivation and activation mechanism of TiO_2 and rGO/Er^{3+}-TiO_2 during flowing gaseous VOCs photodegradation, Appl. Catal. B: Environ. 284 (2021) 119813.